NASA-TM-110498

(NASA-TM-110498) AIRBORNE IMAGING OF TROPOSPHERIC EMISSION AT MILLIMETER AND SUBMILLIMETER WAVELENGTHS (NASA. Goddard Space Flight Center) 3 p

AIRBORNE IMAGING OF TROPOSPHERIC EMISSION AT MILLIMETER AND SUBMILLIMETER WAVELENGTHS

A.J. Gasiewski and D.M. Jackson
School of Electrical and Computer Engineering
Georgia Institute of Technology
Atlanta, GA 30332-0250

J.R. Wang and P.E. Racette
NASA Goddard Space Flight Center
Greenbelt, MD 20771

D.S. Zacharias
ZAX Millimeter Wave Corporation San Dimas, CA 91773

IN-46-TM
39385
3P
N95-24336
Unclas
G3/46 0039385

ABSTRACT

In September 1993, the NASA Millimeter-wave Imaging Radiometer (MIR) flew on board the NASA ER-2 high-altitude aircraft during CAMEX, and obtained the first wideband millimeter- and submillimeter-wavelength images of tropospheric emission. The MIR is a cross-track scanning radiometer with channels at 89, 150, 183±1, 3, 7, 220, and 325±1, 3, 8 GHz. This set provides upwelling brightness information at the two strong rotational water vapor lines at 183.310 and 325.153 GHz and three nearby atmospheric transmission windows. The wideband MIR images of convective raincells reveal unique cloud and precipitation mapping capabilities that are not available from lower frequency microwave channels. Comparisons between the 183 and 325 GHz spectra also reveal differential brightness temperature modes that are related to cloud water.

INTRODUCTION

Satellite-based imaging of atmospheric clouds and water vapor has been successfully performed using both microwave (e.g., the DMSP SSM/I and SSM/T-2 microwave instruments and the NOAA MSU instrument) and IR and visible channels (e.g., the visible and IR imagers on the NOAA geostationary and polar orbiting satellites). Historically, frequencies between the microwave and IR bands have received little attention for at least two reasons: (1) The development of technology for sensitive radiometers at millimeter-wave (MMW) and submillimeter-wave (SMMW) frequencies has lagged such developments at both the lower microwave and visible/IR bands and (2) The opacity caused by water vapor and clouds is relatively large at MMW and SMMW frequencies and has prompted concern that practical nadir imaging of the tropospheric meteorological phenomena would be precluded. However, as discussed by Gasiewski (1992), the potential benefits of satellite-based MMW and SMMW radiometry include high spatial resolution using antennas of practical size and additional spectral information related to the underlying cloud and water vapor state. Accordingly, an investigation into tropospheric imaging using MMW and SMMW bands is underway. In this paper, we report the development and successful deployment of the first wideband MMW and SMMW radiometer for tropospheric cloud, precipitation, and water vapor imaging.

The instrument used is the Millimeter-Wave Imaging Radiometer (MIR), developed by the NASA Goddard Space Flight Center, Georgia Institute of Technology, and ZAX Millimeter Wave Corporation (Racette et al., 1994). The MIR is a total-power cross-track scanning radiometer with channels at 89, 150, 183±1, 3, 7, 220, and 325±1, 3, 8 GHz. The instrument is configured for flight on the NASA ER-2 high-altitude aircraft. All channels are linearly polarized and have identical 3.5° 3-dB beamwidths resulting in 1.2-km spots on the surface at nadir. Cross-track sampling and scan rates are set to provide nadir spatial sampling at ~ 82% of the Nyquist rate or more than twice the commonly used 3-dB spatial sampling rate. Detection is accomplished using five waveguide-fed mixers with integrated antennas. Each mixer is pumped by a Gunn diode local oscillator; both fundamental and harmonic mixers are used. The sensitivity for ~ 30 msec integration time is ~ 0.2 – 0.3 K for the 89- through 220-GHz channels and ~ 1.5 K for the 325-GHz channels. Calibration is accomplished using pyramidal hot and cold blackbody standards. Absolute accuracy is ~ 1 – 2 K for all channels.

The MIR was deployed on the ER-2 during CAMEX (the Convective Atmospheric Moisture Experiment), September-October 1993, during which all nine MMW and SMMW channels were operational. Flights over non-precipitating clouds, convective precipitation (both continental and maritime), and clear-air yielded the first wideband MMW and SMMW tropospheric imagery. This wideband MIR imagery is used here to illustrate several innovative and beneficial applications of high-resolution satellite-based MMW and SMMW observations. These include improvements in measurements of tropospheric water vapor profiles, cloud ice content, rain rate, and raincell extent. The imagery shows that SMMW channels provide unique information pertaining to water vapor density and cloud parameters, either when used alone or in conjunction with lower frequency microwave channels.

CLEAR-AIR SPECTRAL FEATURES

Calculations by Gasiewski (1992) suggested that clear air spectral variations in channels near the 183.310 and 325.153 GHz water vapor lines should be quite similar; hence, spectral differences between these bands should be largely independent of water vapor variations. This hypothesis was investigated by comparing clear-air spectral differences observed during different flights and thus, for different water vapor states. The spectral differences are defined by

$$\Delta T_{183-325} \triangleq \overline{T}_{183} - \overline{T}_{325}$$

where:

$$\overline{T}_{183} = [T_{183\pm1}, T_{183\pm3}, T_{183\pm7}, T_{150}]$$
$$\overline{T}_{325} = [T_{325\pm1}, T_{325\pm3}, T_{325\pm8}, T_{220}]$$

Clear-air data from two flights (sorties #93-164 on September 17, 1993 and #93-168 on September 26, 1993) were examined to check for this behavior (Table1). The average clear-air brightness changes between 9/17/93 and 9/26/93 ranged from 8-16 K for the channels being considered. However, the spectral differences between the 183- and 325-GHz bands varied by no more than 5.5 K, with typical variations of ~ 1 K. With the exception of the 183±1-325±1 difference the data show exceptional rejection of water vapor variations. The relatively large variation (60%) in $T_{183\pm1} - T_{325\pm1}$ is partly due to noise in the 325 ± 1-GHz channel.

PRECEDING PAGE BLANK NOT FILMED

Table 1: Clear-air brightness variations between flights on 9/17/93 and 9/26/93.

	$\Delta T_{183-325}$ 9/17/93 (K)	$\Delta T_{183-325}$ 9/26/93 (K)	Difference (9/17/93-9/26/93) (K)	Difference (9/17/93-9/26/93) (%)
±1	-4.0	-9.6	5.5	60.0
±3	9.3	8.7	0.6	4.7
±7 or ±8	17.5	16.2	1.3	8.4
150 or 220	1.1	1.2	-0.1	0.9

It has also been suggested (Gasiewski 1992) that the large separation in frequency between the 183- and 325-GHz bands (approximately one octave) should result in significantly different responses to small cloud particles. Thus, clouds could be detected and distinguished from water vapor variations by thresholding the $\Delta T_{183-325}$. To this end, we have demonstrated a raincell and cloud detector using the 183-325 GHz spectral differences that is highly invariant to the underlying water vapor state. An optimized version of such a dual-band detector would be extremely useful in removing the effects of thin clouds on 183-GHz water vapor retrievals.

CLOUD AND PRECIPITATION MAPPING

Strip-map images of isolated convective precipitation cells over the Atlantic ocean are shown in Fig. 1. Although the 325-GHz channels are somewhat noisy, the capability to map raincells in this band with high contrast can be clearly seen. The low brightness temperatures (as low as 130 K) over cell cores are the result of scattering of the cold cosmic background flux from ice particles in the cell top. Many weak cells and clouds that escape detection at 89 GHz are clearly outlined in the 325-GHz channels, and to a lesser extent in the 183- and 220-GHz channels.

The responses of the 183-, 220-, and 325-GHz channels to clouds and raincells are monotonic under the prevailing summer midlatitude humidity conditions and ocean surface state. The high zenith opacity of water vapor, low ocean reflectivity, and high values of cloud scattering and absorption at 183, 220, and 325 GHz result in a characteristic cooling signature. This is unlike the 89-GHz channel (and to some extent, the 150-GHz channel), which exhibits a bimodal response to maritime clouds. Thin clouds cause a warming at 89 GHz by increasing the opacity of the reflected path to cold space; heavy clouds and raincells with ice canopies cause strong scattering of the cold background flux. Although reflectivities of dense ice canopies at frequencies near ~ 100 GHz can exceed 60% (Gasiewski and Staelin, 1990), many thin clouds are undetectable at 89 GHz.

Fig. 2 is a scatterplot of the nadir brightness values in Fig. 1 for the 89- and 325±8-GHz channels. The 325±8-GHz values are all lower than the clear-air value of ~ 254 K. The non-monotonic behavior of the 89-GHz channel results in a distribution of points both above and below the clear-air value of ~ 250 K. Such scatterplots show no evidence of saturation of the 325-GHz channels, even at the cell cores. The apparent lack of saturation suggests that these channels can provide a wide dynamic brightness temperature range for purposes of cloud and raincell detection and parameter estimation. Further, the large brightness variations (up to ~ 150 K) in the 325-GHz channels indicate that these channels are not seriously screened by water vapor, and exhibit useful sensitivity to clouds and raincells having moderate ($\sim 5-7$ km) top altitudes. As expected for spectral line imagery, the amplitude of the cloud-top scattering signature in the 325-GHz channels increases as the channel frequency shifts away from the line center.

WIDEBAND RAINCELL SPECTRA

Raincells are best observed using radiometric channels centered in the atmospheric transmission windows. Although storm intensity and rain rate are correlated with MMW and SMMW

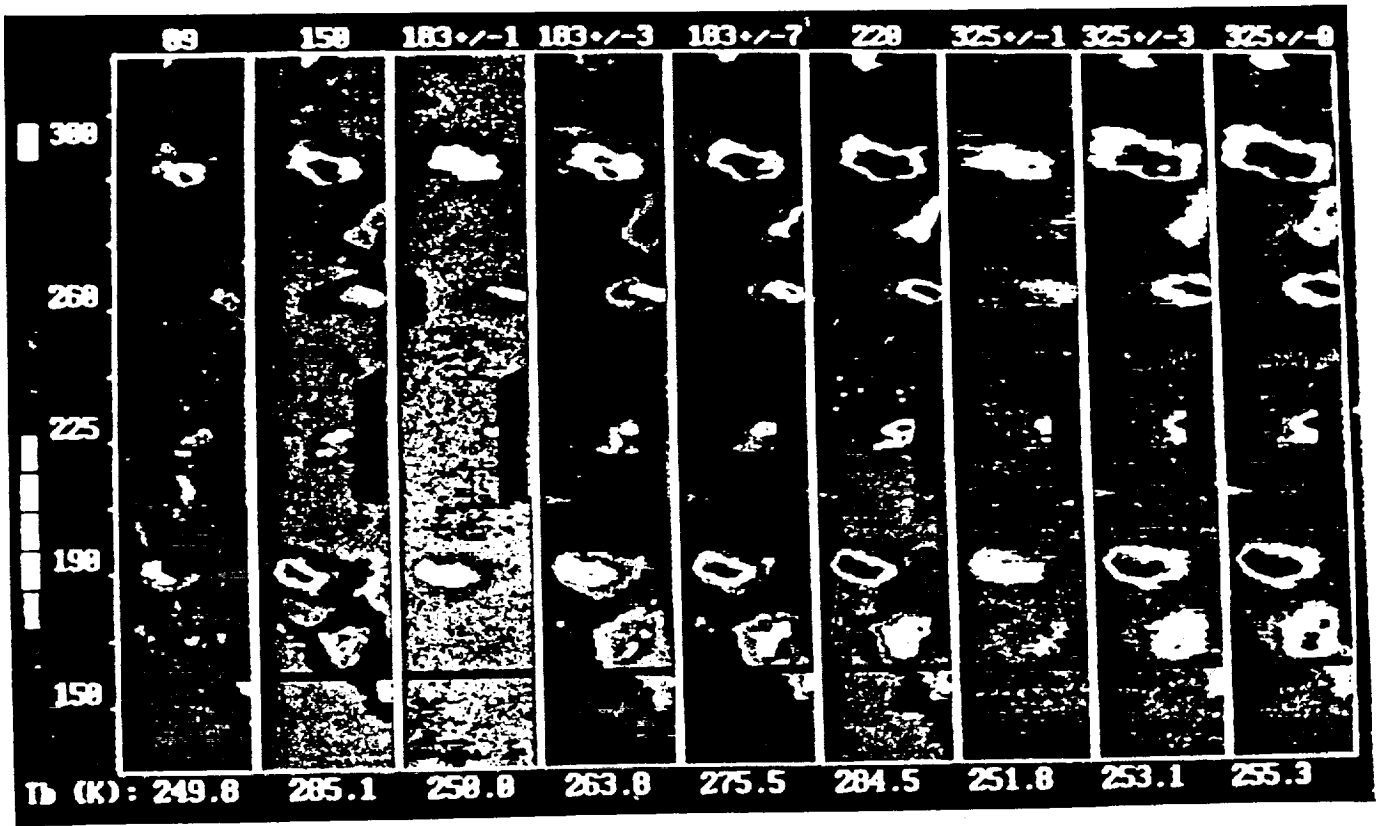

Figure 1: Strip map images of upwelling thermal emission from isolated convective cells over ocean (September 27, 1994). Each map covers approximately 40 x 220 km; cells are distorted slightly due their proximity to the aircraft. Average clear-air brightness temperature values at nadir are indicated below each map.

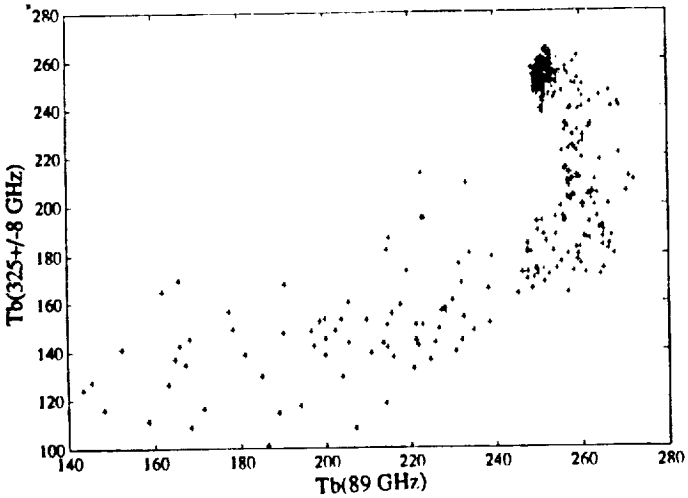

Figure 2: Scatterplot of nadir brightness temperatures over oceanic convection for the MIR 89- and 325±8-GHz channels (September 26, 1994).

window-channel brightness variations, the parameter most directly related to these variations is the vertically integrated ice content (IIC) in the cell top. The IIC is, in turn, highly correlated with the reflectivity of the cell top, and hence, the upwelling brightness temperature. Statistical retrieval of IIC from MMW observations at frequencies up to ~ 90 GHz using the dominant spectral modes of the raincell brightness temperatures appears feasible, although IIC retrieval algorithms are difficult to validate from field experiments.

The high sensitivity of the MIR's MMW and SMMW channels to IIC are expected to further facilitate such IIC estimates. As shown by the nadir lineplot (Fig 3) the MIR window channels at 89, 150, 220, and 325±8 GHz all provide large responses to the ice canopies over raincells. The strength of these responses can be analyzed using the Karhunen-Loève (KL) transform (Gasiewski and Staelin, 1989), computed as:

$$\overline{k} = \overline{\overline{E}}^{t} \, \Delta\overline{T}_B$$

where $\overline{\overline{E}}$ is an orthogonal column matrix containing the eigenvectors of the brightness temperature covariance matrix and $\Delta\overline{T}_B$ is the brightness temperature referenced to clear air. From the data, the dominant spectral mode is found to have close to the same contributions from all four channels, indicating that these channels exhibit comparable variance from ice. This mode has a signal-to-noise ratio (SNR) greater than ~ 35 dB for the MIR rain cell observations in Fig 3.

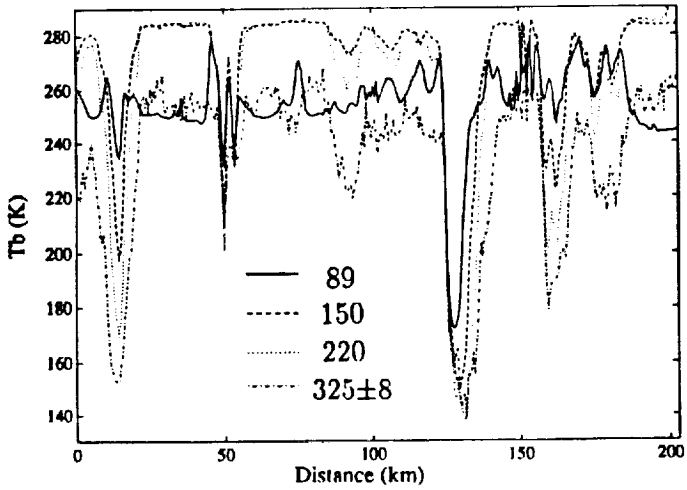

Figure 3: Brightness temperatures observed at nadir for the four MIR window channels at 89, 150, 220, and 325±8 GHz. Plots are for the same overflight as in Fig. 1.

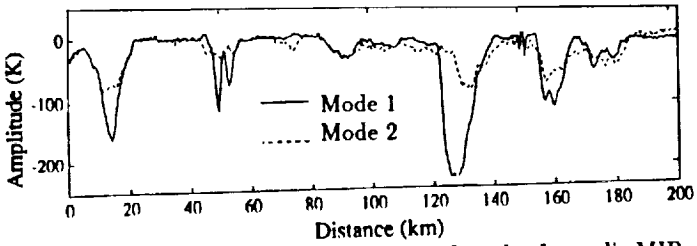

Figure 4: Two most dominant KL spectral modes for nadir MIR window channel observations over raincells. Plots are for the same overflight as in Fig. 1.

However, there are at least two other modes in the window channel data that exhibit SNR's greater than 10 dB. The second most energetic mode is the difference between the high- and low-frequency window channels; thus, it filters the slope of the raincell spectrum. This mode varies independently of the first mode as seen in Fig. 4 between 120 and 140 km. Although meaningful relationships between the KL modes and physical raincell parameters are not guaranteed, it appears that the second KL mode responds to radiometrically thin portions of the cell, in particular, the anvil regions. Indeed, because of the relatively flat spectrum of hydrometeor absorption and scattering, it is desirable to observe raincells using several channels that are widely separated in frequency. The MIR channels at 89, 150, 220, and 325±8 GHz provide such wideband measurements, spanning nearly two octaves in frequency.

CONCLUSIONS

The MIR data obtained during CAMEX show that simultaneous use of the two water vapor bands near 183 and 325 GHz offers a viable means of both improving spaceborne passive measurements of cloud water content and of discriminating between clouds and water vapor in passive retrievals. The 325-GHz channels alone show potential for cloud and midlatitude raincell mapping without saturation or excessive water vapor screening. These channels are expected to be useful for high-resolution cloud parameter estimation and provide an improved means of monitoring global cloud water content. When used in conjunction with other MMW and SMMW window channels, the 325-GHz channels provide unique information on the hydrometeor distribution through additional spectral degrees of freedom. While this initial analysis appears very promising, it is noted that the observations were performed only under summer midlatitude conditions. Additional observations are desirable under a variety of baseline meteorological conditions for a complete characterization of the available MMW and SMMW channels.

ACKNOWLEDGEMENTS

The authors would like to thank Dr. Ramesh Kakar at NASA Headquarters for his support of the MIR, and Scott J. Sharpe at the Georgia Institute of Technology for assistance in the MIR data processing. This work was supported by NASA grant NAG 5-1490 and the Georgia Tech Research Corporation.

REFERENCES

Gasiewski, A.J., and D.H. Staelin, "Statistical Precipitation Cell Parameter Estimation Using Passive 118-GHz O_2 Observations," *J. Geophys. Res.*, vol. 94, no. D15, pp. 18367-18378, December, 1989.

Gasiewski, A.J., and D.H. Staelin, "Numerical Modelling of Passive Microwave O_2 Observations Over Precipitation," *Radio Sci.*, vol. 25, no. 3, pp. 217-235, 1990.

Gasiewski, A.J., "Numerical Sensitivity Analysis of Passive EHF and SMMW Channels to Tropospheric Water Vapor, Clouds, and Precipitation," *IEEE Trans. Geosci. Remote Sensing*, vol. 30, no. 5, pp. 859-870, September 1992.

Racette, P.E., R.F. Adler, A.J. Gasiewski, D.M. Jackson, J.R. Wang, and D.S. Zacharias, "An Airborne Millimeter-Wave Imaging Radiometer for Cloud, Precipitation, and Atmospheric Water Vapor Studies," submitted to *J. Atmos. Oceanic Tech.*, February 1994.